AIAA JOURNAL
Vol. 33, No. 10, October 1995

Reduction of Fluctuating Pressure Loads in Shock/Boundary-Layer Interactions Using Vortex Generators

J. W. Barter* and D. S. Dolling†
University of Texas at Austin, Austin, Texas 78712

Fluctuating wall pressure measurements have been made in a separated shock wave/turbulent boundary-layer interaction produced by an unswept compression corner in a Mach 5 flow. Wheeler doublet vortex generators were placed upstream of the corner to study their effect on the fluctuating pressure loads within the interaction. The vortex generators produce significant three dimensionality in an otherwise two-dimensional interaction. They reduce the upstream influence and the length of the region of separation shock motion by 60% and 64%, respectively, and they decrease the maximum wall pressure rms near separation by 23% and shift the fluctuations to higher frequencies. The maximum fraction of energy in the resonant frequency band of typical skin panels (i.e., 100–500 Hz) is decreased by 11%. On the corner face, where the maximum loads occur, the maximum wall pressure rms is reduced by 10%, and the maximum fraction of energy in the 100–500 Hz band is reduced by 35%. These changes are due to a fuller boundary-layer profile, a weaker separation shock, increased boundary-layer turbulence causing increased separation shock jitter, and a shorter region of shock motion.

Nomenclature

C_f = skin friction coefficient
f = frequency
f_c = separation shock zero crossing frequency
$G(f)$ = spectral density function
L_i = intermittent region length
P = pressure
Re_θ = Reynolds number based on momentum thickness
T = temperature, separation shock period
U = velocity
X = streamwise distance normalized by δ, Fig. 1
Y = spanwise distance normalized by δ, Fig. 1
Z = vertical distance normalized by δ, Fig. 1
β = fraction of wall pressure variance in the 100–500 Hz band
δ = undisturbed boundary-layer thickness
δ^* = undisturbed boundary-layer displacement thickness
γ = wall pressure signal intermittency
θ = undisturbed boundary-layer momentum thickness
Π = undisturbed boundary-layer wake strength parameter
σ = standard deviation

Subscripts

max = maximum value
pw = wall pressure
rms = root mean square value
t = pitot pressure
vg = vortex generator
w = wall
∞, inf = freestream condition
0 = stagnation quantity

Introduction

IT is well known that when a shock wave of sufficient strength interacts with a boundary layer it can cause separation. In the case of shock-induced turbulent boundary-layer separation the process is unsteady. Interaction unsteadiness produces large-amplitude fluctuating pressure loads as high as 185 dB,[1] which can substantially shorten the fatigue life of vehicle components. These high loads occur near separation and reattachment, and under the outgoing boundary layer, and are largely caused by fluctuations in the instantaneous positions of separation and reattachment. The frequency band of the highest amplitude loads is typically in the range from several hundred hertz to several kilohertz. This band exacerbates the loading problem because the resonant frequency band for typical skin panels is 100–500 Hz. Predictions for a transatmospheric vehicle suggest that the time to failure of advanced metal matrix composite structures under such loading is typically on the order of minutes.[2]

The separated flow produced by shock wave/turbulent boundary-layer interactions (SWTBLIs) can also substantially reduce aerodynamic efficiency. Consequently, many previous attempts to control these interactions have focused on either eliminating separation or reducing the total pressure loss through the shock.[3–7] In light of the effect of shock wave/turbulent boundary-layer interactions on structural fatigue, some recent control studies have focused on fluctuating loads reduction. McClure[8] explored a number of techniques, including boundary-layer manipulators and riblets, with limited success. Kleifges and Dolling[9] had greater success using a swept root fillet to reduce the loads produced in an unswept blunt fin-induced interaction.

The objective of the current study is to explore ways to reduce fluctuating pressure loads in SWTBLIs to extend fatigue life. It is hoped that through changes in the separation shock dynamics (and reattachment process), the magnitude of the loading can be reduced, its spectral content altered, and the area exposed to high loads reduced. In this paper, the effects of Wheeler[10] doublet vortex generators (VGs) are examined.

Previous experiments have shown that vane type vortex generators are ineffective in controlling shock-induced turbulent boundary-layer separation.[11] Wheeler doublets are better suited for this application because they, unlike vane VGs, do not produce shocks that impinge on the interaction. Rather, provided that the doublets are sufficiently far upstream, the VG leading-edge shocks pass over the interaction. Each Wheeler doublet produces a pair of counter-rotating vortices that energize the boundary layer by transferring high-momentum fluid from the outer region of the boundary layer to the inner region. Low-momentum fluid swept from under the vortices collects between the counter-rotating pair. In the case of the Wheeler doublets, this produces a relatively low-momentum region downstream of the VG apexes.[12] Barber et al.[13] conducted a computational, parametric study of Wheeler doublets to determine the geometry that best energizes the boundary layer. In this study, the incoming flow was inviscid and subsonic and a $\frac{1}{7}$ power law velocity

Received July 23, 1994; revision received Jan. 3, 1995; accepted for publication Jan. 19, 1995. Copyright © 1995 by the American Institute of Aeronautics and Astronautics, Inc. All rights reserved.

*Graduate Research Assistant, Department of Aerospace Engineering and Engineering Mechanics, Center for Aeromechanics Research. Student Member AIAA.

†Professor, Department of Aerospace Engineering and Engineering Mechanics, Center for Aeromechanics Research. Associate Fellow AIAA.

profile was used to simulate an incoming turbulent boundary layer with a thickness that was three times the VG height. The code was validated and calibrated for a single VG geometry with experiments conducted in a low-speed wind tunnel. Of the geometries examined numerically, their results indicate that a length:width:height ratio of 6:5:1 is best, although this result may not be accurate for high speed flows.

The selection of Wheeler doublets for exploring interaction control stems from observations made in previous studies. McCormick[14] placed Wheeler doublets upstream of a normal shock/turbulent boundary-layer interaction and used surface flow visualization and mean pressure measurements to study their effect on the mean interaction. His results show that the length scale of the interaction was reduced by the VGs. Although McCormick did not address interaction unsteadiness, his results suggest that the intermittent region (i.e., the region of separation shock motion) is shorter as compared to the undisturbed interaction. This inference is based on observations from other studies that have shown that the intermittent region spans the region from the upstream influence line (UI) to the separation line (as determined from the mean pressure distribution and surface tracer patterns). Gonsalez and Dolling[15] have also observed that in a given boundary layer the mean velocities of the unsteady separation shock are independent of the intermittent region length; thus, with a smaller intermittent region, shock frequencies increase. These two observations suggested that the placement of Wheeler doublets upstream of an interaction would shift separation shock motion to a higher frequency band through shortening of the intermittent region. This is turn should shift the fluctuating pressure loads to a higher frequency band.

Experimental Program

Wind Tunnel and Flow Conditions

All experiments were conducted in the Mach 5 blowdown wind tunnel at the University of Texas at Austin. Barter and Dolling[16] describe this facility. The test section used for these experiments is 68.6 cm (27 in.) long, 15.2 cm (6 in.) wide, and 17.8 cm (7 in.) high. All tests were conducted with the models mounted on the test section floor. The floor boundary layer undergoes natural transition upstream of the nozzle and develops under approximately adiabatic wall temperature conditions. Values of the stagnation and freestream properties, and boundary-layer parameters measured in the undistributed flow approximately 1δ upstream of the compression corner location are listed in Table 1. The values for the boundary-layer parameters listed in this table are nominal on the tunnel centerline. There are systematic spanwise variations in the boundary-layer parameters which are probably due to Taylor–Gortler vortices in the boundary layer.[17] The variations in $\delta, \delta^*, \theta, C_f$, and Re_θ are $\pm 4.5\%$, $\pm 8.3\%$, $\pm 6.2\%$, $\pm 6.0\%$, and $\pm 6.2\%$, respectively. Changes in the stagnation pressure controller settings from one experimental phase to another resulted in the uncertainty of P_0 being $\pm 0.9\%$, $\pm 0.6\%$, and $\pm 3.0\%$ for fluctuating wall pressure measurements, pitot surveys of the boundary layer upstream of the interaction, and pitot surveys above the compression corner face, respectively.

Models

The interaction was generated by a 28-deg unswept compression corner. This particular interaction was selected because it produces a nominally two-dimensional flowfield that has been studied in detail in this facility.[8,18,19] The model is 6.25δ wide and 1.97δ high, and it can be adjusted streamwise relative to a fixed row of transducers upstream. This model, with the Wheeler doublets upstream, is shown in Fig. 1. Fences, 0.16δ thick, were attached to the model to prevent spillage and to isolate it from the tunnel side-wall boundary layers. The leading edges of the fences were beveled to prevent shocks from interfering with the interaction. The fences extended 3.95δ upstream of and 1.32δ above the compression corner model.

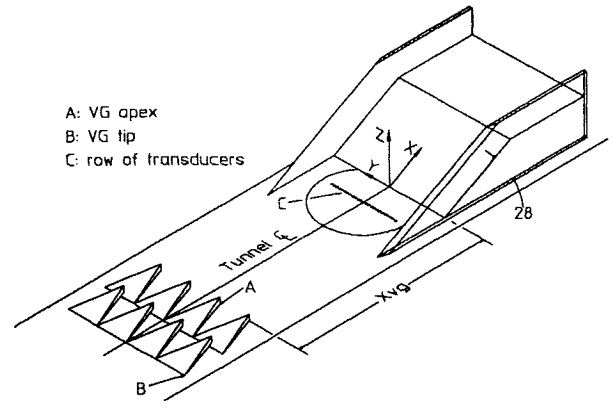

Fig. 1 Model with 28-deg unswept compression corner with VGs upstream.

To acquire fluctuating pressure loads data on the corner face, an instrumented compression corner model was also used. The face of this model has a single row of transducer ports along its centerline and can be slid in and out of the tunnel floor so that the streamwise positions of the transducers can be adjusted. This model is 4.61δ wide and 2.16δ high. Beveled fences, 0.25δ wide, were again attached to the sides of the model and, as before, they extended 3.95δ upstream of and 1.32δ above it.

An array of four Wheeler doublets was placed 15.8δ ($X_{vg} = -15.8$) upstream of the compression corner as shown in Fig. 1. In a preliminary set of experiments, VG positions in the range $-21 \leq X_{vg} \leq -11$ were examined. No significant variations in the intermittent region flowfield were observed as the variations of σ_{pw} and f_c were less than 5% when comparing equivalent locations in the intermittent region. Therefore, it was concluded that within the range $-21 \leq X_{vg} \leq -11$, the position of the VGs has only a second-order effect on the separation shock dynamics. Each doublet is made of two Wheeler singlets placed in line. McCormick's results[14] indicate that the doublet arrangement is more effective than the singlet in perturbing the mean interaction scale; therefore, the doublet arrangement was used exclusively. Each singlet is 0.33δ high, 2.37δ long, and 1.64δ wide. This ratio of length to width to height was selected to match that used by McCormick[14] because, at the time these experiments were begun, the computational results of Barber et al.[13] were not available. When placed in line, each singlet overlapped the downstream one by 0.26δ (see Fig. 1) giving a total doublet length of 4.47δ.

The VGs were attached to the tunnel floor using Devcon® instant adhesives super glue. To ensure that the spanwise placement of the VGs was repeatable, a template was used to place them in the desired arrangement. During tests in which wall pressure data were taken on the tunnel floor, it was necessary to move the compression corner model to make measurements at various locations in the intermittent region. As a result, there is a $\pm 1.7\%$ variation in X_{vg}. Based on the experiments just cited, the effects of such a shift in X_{vg} are judged negligible.

Table 1 Freestream flow conditions and turbulent boundary-layer properties

Parameter		
M_∞	4.92 ± 0.02	
P_0, MPa (psia)	2.34	(340)
T_0, K(°R)	356 ± 2.8	(640 ± 5.0)
U_∞, m/s (ft/s)	771 ± 4.3	(2530 ± 14)
δ, cm (in.)	1.93	(0.76)
Re_θ	3.9×10^4	
δ^*, cm (in.)	0.90	(0.36)
θ, cm (in.)	0.075	(0.03)
$C_f \times 10^3$	0.76	
Π	0.44	

Instrumentation and Data Acquisition

Wall pressure measurements were made using Kulite® model XCQ-062-15A (0–15 psia) and XCQ-062-50A (0–50 psia) transducers. The outside diameter of these transducers is nominally 0.16 cm (0.0625 in.). The pressure sensing element is a 0.071-cm- (0.028-in.-) diam silicon diaphragm with a Wheatstone bridge atomically diffused into it. With their protective screens in place,

these transducers have a frequency response of about 50 kHz when mounted flush with the tunnel wall. The output of the transducers was amplified and low-pass filtered at a cutoff frequency of 50 kHz to prevent aliasing. The typical signal to noise ratio was about 100. The transducers were installed either in a 8.57-cm- (3.375-in.) diam circular instrumentation plug that could be inserted flush with the tunnel floor (Fig. 1) or in the instrumented compression corner model. When transducer ports were not being used, they were filled with dummy plugs. To insure that the transducers and dummy plugs were flush with the instrumentation plug face, the installation was inspected using a magnifying glass.

The instrumentation plug could be rotated such that the transducers were either in a streamwise or spanwise row. Because the undisturbed (or baseline) interaction is nominally two dimensional,[19] it was investigated using transducers placed in a streamwise row. However, the addition of the VGs upstream introduces significant three dimensionality into the incoming boundary layer. Therefore, when investigating the disturbed interaction, the transducers were placed in a spanwise row so that the effects of this three-dimensional boundary layer could be ascertained.

To measure fluctuating loads on the corner face, the instrumented, unswept compression corner model was used. With this model it was not possible to place the transducers in off-centerline locations; therefore, to assess the spanwise effects of the VGs, the VGs were moved spanwise relative to the fixed instrumented model. By moving the VGs it was possible to measure the loads on the corner face downstream of VG apex, tip, and midspan (i.e., the location halfway between the apex and tip).

Mean pitot pressure surveys were also made of the incoming boundary layer using a pitot rake with seven tubes in a spanwise row. Individual tips were 1.27 cm (0.5 in.) apart. The rake could be shifted 0.64 cm (±0.25 in.) spanwise such that the boundary layer can be studied up to 4.45 cm (±1.75 in.) off centerline. Because of geometric limitations, measurements could not be made below $Z = 0.013$. The pitot pressure measurements were made using Kulite CTQH-187-50A transducers which are located inside the rake approximately 6.35 cm (2.5 in.) downstream of the pitot tube tips. The vertical displacement of the pitot rake was measured using a calibrated linear variable differential transformer (LVDT).

It was not possible to use the pitot rake to make measurements above the compression corner face; therefore, a single-tipped pitot probe was used. This probe could only be used along the compression corner's centerline so the VGs were shifted spanwise relative to the model to assess their spanwise effects. Surveys of the boundary layer on the corner face were conducted in the same manner as described for the pitot rake. To account for the variation in the tunnel stagnation pressure, the latter was measured simultaneously with the pitot pressure, and the appropriate value was used during data analysis.

Data Analysis

Besides computing the basic statistical properties of the fluctuating pressure data (mean, standard deviation, power spectrum, etc.), the data taken in the intermittent region were also analyzed to determine the dynamics of the separation shock foot. The algorithm for quantifying the shock dynamics is thoroughly discussed by Brusniak.[20]

In this study, the upstream boundary of the intermittent region (i.e., the upstream influence line) is defined as the location where the intermittency is 1%. Intermittency is the fraction of time that the separation shock is upstream of a given point. Similarly, the downstream boundary ($\gamma = 0.99$ line) is defined as the location where the intermittency is 99%. The distance between these boundaries is the intermittent region length. Erengil and Dolling[21] have shown that the error function is a good fit to the intermittency data. Using a code written by Gonsalez[22] the intermittency data were least-squares curve fit such that the upstream and downstream boundaries of the intermittent region and its length could be systematically determined. A second code written by Gonsalez was used to apply a Fourier series curve fit to the zero crossing frequency data so that $f_{c,\max}$ could also be estimated consistently. The zero crossing frequency is a measure of how often, on average, the separation shock crosses a given point in a given direction, and it can indicate shifts in the dominant frequency band of the wall pressure fluctuations.

To evaluate the VGs' effectiveness in shifting the energy of the wall pressure fluctuations to a higher frequency band, it is necessary to quantify the fraction of the wall pressure variance in a given frequency band. The spectral density function $G(f)$ describes how the mean squared value of the wall pressure is distributed in the frequency domain. The integral of $G(f)$ over a prescribed frequency band divided by the overall variance of the wall pressure gives the fraction of energy β due to wall pressure fluctuations in the frequency band. As discussed earlier, the typical resonant frequency band for aircraft skin panels is 100–500 Hz. The described technique is used to determine the effectiveness of the VGs in decreasing β in this frequency band.

Results

Undisturbed Interaction

A drawing of the undisturbed interaction flow structure is presented by Settles et al.[23] The separation shock motion has been characterized by Erengil and Dolling[24] as having two components. The first is a low-amplitude, high-frequency jitter motion produced by fluctuations in the instantaneous pressure ratio across the separation shock caused by the passage of turbulent structures. This jitter is superimposed upon a large-scale, low-frequency motion largely produced by pulsation of the separated flow. The combination of these two types of motion produces the observed streamwise variation in flow properties.

The wall pressure rms, intermittency, and zero crossing frequency distributions are shown in Fig. 2. The intermittent region is 1.41δ long with upstream influence 2.94δ upstream of the compression corner leading edge. The maximum rms of the wall pressure, normalized by P_∞, and the maximum zero crossing frequency are 0.48 and 0.86 kHz, respectively. The fraction of the overall variance contained in the 100–500 Hz frequency band at all stations in the intermittent region is also shown in Fig. 2. Over the range of $0.1 \leq \gamma \leq 0.85$ about 35% of the total wall pressure fluctuation energy is contained in this band.

Marshall and Dolling[19] studied the spanwise variation of intermittent region properties. Marshall and Dolling's experiment were conducted in the same facility under essentially the same freestream conditions but farther upstream with a thinner boundary layer. Their data were analyzed with the same codes used in the present study. Figure 3 shows the spanwise variation of intermittency obtained using Marshall and Dolling's data. The spanwise variations in this figure are representative of the spanwise variations of the mean

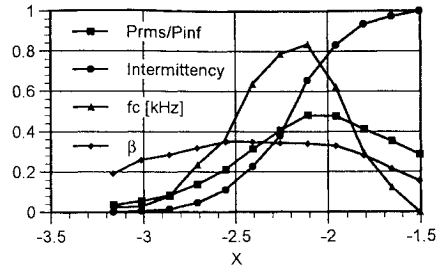

Fig. 2 Wall pressure rms, intermittency, zero crossing frequency, and β distributions in the undisturbed interaction.

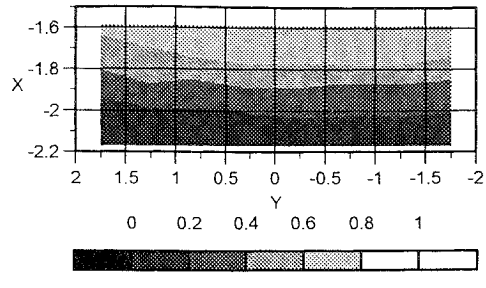

Fig. 3 Spanwise variation of intermittency in the undisturbed interaction.

wall pressure and wall pressure rms. It can be seen that the interaction is nominally two dimensional with significant departures from two dimensionality caused by three dimensionality in the incoming boundary layer occurring only at the edges. There is no spanwise periodicity, which is an important distinction between these results and those to be presented later.

Effect of the VGs on the Incoming Boundary Layer

Mean pitot pressure surveys of the boundary layer were made with and without the VGs upstream. Figure 4a shows that the undisturbed boundary layer pitot pressure distribution is essentially uniform spanwise. The velocity profiles derived from these pitot surveys are good fits to law of the wall law of the wake at all spanwise stations.

Pitot pressure measurements were made at two stations downstream of the VGs to obtain an indication of the streamwise development of the disturbed boundary layer. These surveys show that the VGs fill out the velocity profile of the incoming boundary layer in certain regions and produce momentum-deficient regions downstream of the VG apexes. Figure 4b shows the disturbed normalized boundary-layer pitot pressure distribution 6.6δ downstream of the VGs. There is a distinct three-dimensional pattern in the disturbed boundary layer. Downstream of the VG apexes at $Y = \pm 0.82$, there is a dominant low-momentum region which, although not evident in the contour plots, causes a substantial thickening of the boundary layer. These low-momentum regions appear between regions of high-momentum fluid. The pitot pressures in this region are higher (maximum increase: 28%) than those measured at the same location in the undisturbed boundary layer. The near-wall region ($Z < 0.15$) is largely unaffected by the vortex generators. There is little spanwise variation in measured pitot pressure near the wall, and the magnitudes are the same for the undisturbed and disturbed boundary layers.

Pitot pressures measured 14.5δ downstream of the VGs, shown in Fig. 4c, are similar to those seen in Fig. 4b. The most noticeable difference seen in Fig. 4c is that there is a substantial spanwise thinning of the low-momentum regions downstream of the VG apexes. The maximum increase in pitot pressure due to the action of the vortices at this streamwise station is 39% indicating that the vortices are still coherent and acting to fill out the boundary layer between 6.6δ and 14.5δ downstream.

It was mentioned earlier that in preliminary experiments the location of the VGs was found to have only a second-order effect on the separation shock dynamics. The striking similarity between Figs. 4b and 4c indicates why. As the boundary layer travels from 6.6δ to 14.5δ downstream of the VGs its structure does not change substantially. The vortices continue to energize the boundary layer at 14.5δ downstream and do not appear to be moving away from the wall very rapidly. Consequently, these VGs have the potential to be effective over a wide range of streamwise locations.

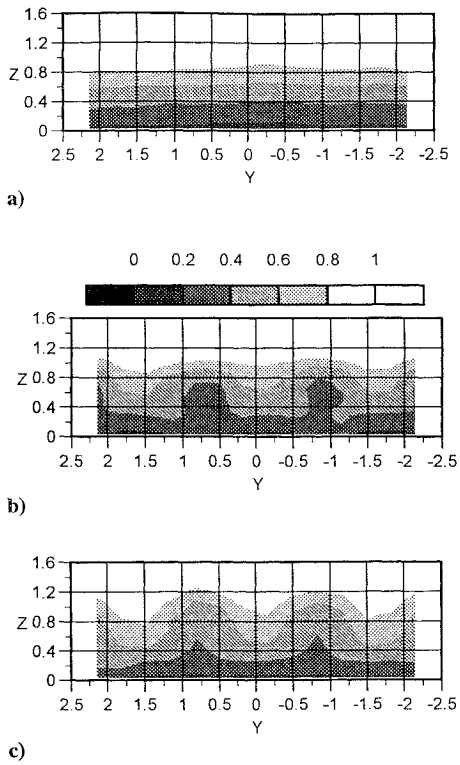

Fig. 4 Boundary layer pitot pressure surveys: a) undisturbed and b) disturbed, measured 6.6δ downstream of the VGs; and c) disturbed, measured 14.5δ downstream of the VGs (normalized by $P_{t,\infty}$).

Effect of the VGs on the Flowfield Scale and Structure

The placement of Wheeler doublet vortex generators upstream of the SWTBLI has a major effect on the size and shape of the flowfield upstream of the corner. Before viewing contour plots of properties in the intermittent region, it is useful to note that the VG apexes were located at $Y \pm 0.82$ and ± 2.47. Also recall that the array of VGs was symmetric about the wind-tunnel centerline ($Y = 0$).

Figure 5 shows surface flow visualization of the disturbed interaction using a kerosene, diesel, lampblack mixture. In this figure, the separation line is labeled S and the leading edge of the compression corner is labeled C. From this figure it is clear that the interaction is three dimensional and spanwise periodic. This periodicity is consistent with the placement of the VGs upstream. The separation line moves upstream in the region directly downstream of the VG apexes and a nearly straight, streamwise, white line appears on the corner face downstream of each apex. It is believed that these lines result from the flowfield being symmetric about streamwise lines through the VG apexes.

Before looking at these spanwise variations in detail, it is possible to make a few general observations about the changes and their relationship to the undisturbed interaction. In the presence of the VGs, the maximum length of the intermittent region is 0.55δ and the maximum upstream influence is 1.16δ. Compared with the undisturbed interaction, these lengths are 60% shorter. The minimum intermittent region length and upstream influence are 0.45δ and 1.10δ, respectively, which are 67% and 62% shorter than in the undisturbed interaction.

Figure 6 shows the intermittency distribution through the interaction. On the basis of repeated measurements, the uncertainty of the intermittency is estimated to be 5%. The VGs make the interaction spanwise periodic, and this periodicity in the intermittency distribution is consistent with the results of the flow visualization shown in Fig. 5. The initial rise in intermittency first occurs in the regions of the interaction downstream of the VG apexes. This indicates

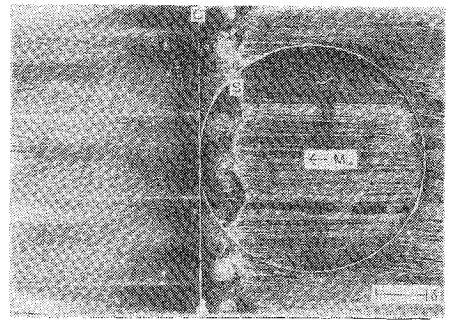

Fig. 5 Surface flow visualization of the disturbed interaction.

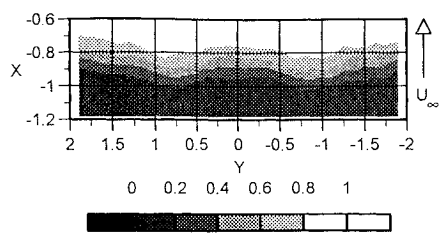

Fig. 6 Intermittency distribution.

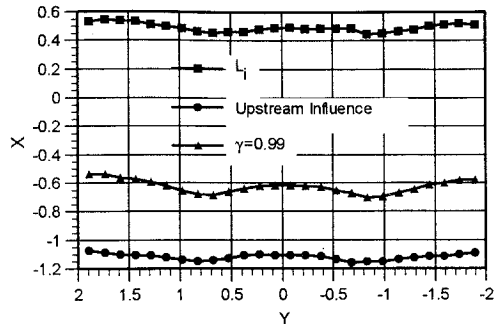

Fig. 7 Spanwise variation of intermittent region length, upstream influence, and $\gamma = 0.99$ line.

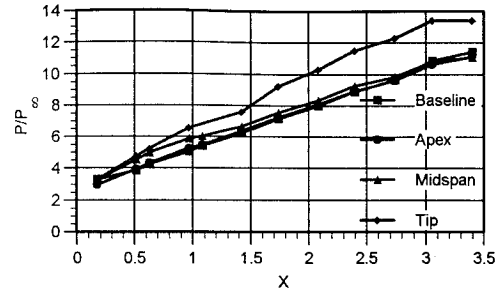

Fig. 8 Mean pressure distributions along the corner face.

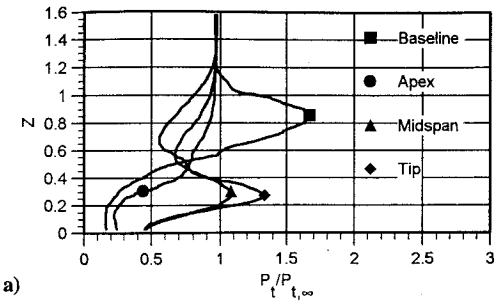

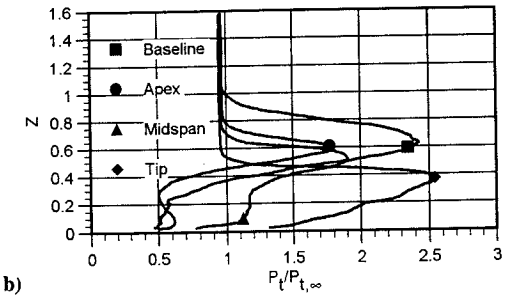

Fig. 9 Pitot pressure surveys above the corner face: a) $X = 1.5$ and b) $X = 2.24$.

that the VGs are least effective in the region downstream of their apexes, which is to be expected as the counter-rotating vortices deposit low-momentum fluid in this region. The effect of the VGs increases away from the apexes. In the region between the apexes ($-0.82 \leq Y \leq 0.82$) the initial rise in pressure and intermittency moves downstream. Outside the apexes at $Y = \pm 0.82$, the intermittent region moves farther downstream due to nonuniformities in the incoming boundary layer.

The downstream shift of the intermittent region outside the VG apexes is consistent with the shift observed in the undisturbed interaction. It was previously shown in Fig. 3 that as the distance from the tunnel centerline ($Y = 0$) increases, the interaction becomes increasing three dimensional. Figure 3 shows that the departure from two dimensionality is greatest on the left side ($Y > 0$) of the tunnel. Similarly, Fig. 6 shows that the left side of the tunnel has a greater downstream shift than the right side of the tunnel. In the following discussion, the regions outside the first set of apexes ($Y = \pm 0.82$) will be shown in the figures to demonstrate the spanwise periodic structure of the interaction. However, to avoid effects due to three dimensionality in the undisturbed tunnel floor boundary layer, only the region between the apexes will be considered when evaluating the effectiveness of the VGs in reducing fluctuating pressure loads.

Spanwise variation of the intermittent region length and upstream influence and $\gamma = 0.99$ lines were computed from the intermittency data. Details regarding the computation of these curves are given by Barter and Dolling.[16] The spanwise variations of the intermittent region length, upstream influence, and $\gamma = 0.99$ line are shown in Fig. 7. The spanwise variations of these lengths are spatially periodic which is consistent with the previously observed results. The minimum and maximum intermittent region lengths are approximately 0.45δ and 0.49δ (when only considering the region between VG apexes). This spanwise variation of L_i is remarkably small when one considers the magnitude of the variations in the incoming boundary layer. The minima occur downstream of the VG apexes whereas the maximum is located along the line of symmetry between the VGs.

The observed variations in L_i are driven by variations in both the upstream influence and $\gamma = 0.99$ lines. The upstream influence line is nearly straight with small shifts upstream in the regions downstream of the VG apexes. Like UI, the $\gamma = 0.99$ line shifts upstream in the region downstream of the VG apexes. However, the shift in $\gamma = 0.99$ is greater than that of UI and as a result, the intermittent region becomes smaller downstream of the VG apexes.

On the corner face, the flow structure is also highly three dimensional as demonstrated by the mean pressure distributions along the face shown in Fig. 8 and the pitot pressure profiles shown in Fig. 9. Downstream of the VG tips, the flow is compressed much more quickly than is observed in the undisturbed flow and, as a result, pressure gradients in the spanwise direction exist on the face that cause fluid to move from the VG tips toward the apex. It is difficult to interpret the pitot pressure distributions because the local total pressure and Mach number vary in the streamwise and spanwise directions. However, these profiles do appear to confirm that there is significant spanwise flow along the corner face that fills out the velocity profile in the region downstream of the VG apex.

Effect of the VGs on Fluctuating Pressure Loads in the Intermittent Region

The vortex generators have two effects on the fluctuating pressure loads produced by the SWTBLI. First, the magnitude of the maximum wall pressure rms is reduced. Second, the frequency range of the fluctuating loads in the disturbed interaction is shifted to a higher band. Figure 10 shows the wall pressure rms in the intermittent region. On the basis of repeated measurements, the experimental uncertainty of σ_{pw} is estimated to be 4%. Like the intermittency distribution, the wall pressure rms distribution is spatially periodic, and this periodicity is consistent with the locations of the vortex generators upstream. Root mean square levels first rise above the turbulent boundary-layer level downstream of the VG apexes. The highest rms levels occur between the VG apexes near the downstream edge of the interaction. The maximum σ_{pw}/P_∞ is 0.37, which is a decrease of 23% compared to the undisturbed interaction. The peak rms downstream of the apexes is slightly lower at 29% below the undisturbed interaction peak rms. This reduced σ_{pw}/P_∞ is due to a smaller separated flow having a weaker separation shock, as shown by the fact that in the disturbed interaction $\overline{P}_w/P_\infty$ at $\gamma = 0.99$ is 0.15 to 0.25 less than that observed in the undisturbed interaction.

The zero crossing frequency distribution in the intermittent region is shown in Fig. 11, and it too is periodic. The experimental uncertainty is estimated to be 15%. The overall maximum zero crossing frequency is 2.33 kHz, which is a 171% increase over $f_{c,\max}$ in the undisturbed interaction. As with undisturbed interaction, the maximum zero crossing frequency occurs near 50% intermittency.

The shift to higher zero crossing frequencies is due to enhanced jitter type motion of the separation shock. Shown in Fig. 12 are

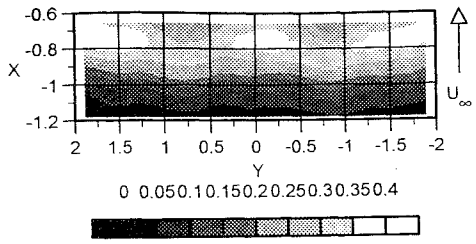

Fig. 10 Wall pressure rms distribution in the intermittent region, normalized by P_∞.

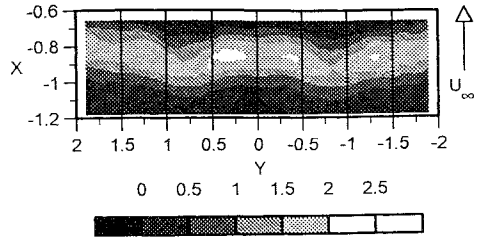

Fig. 11 Zero crossing frequency (kHz) distribution in the intermittent region.

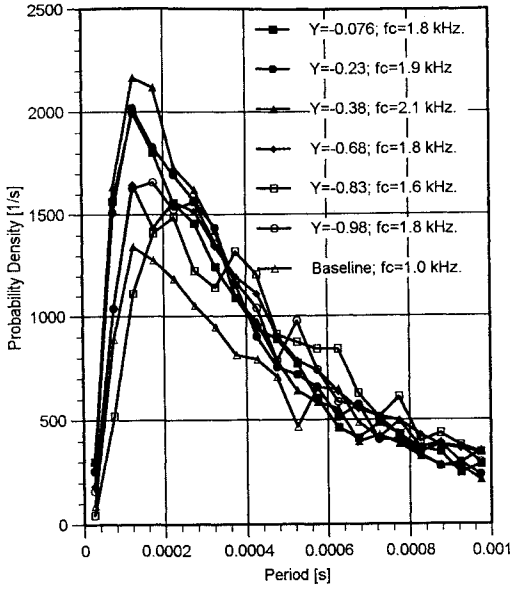

Fig. 12 Spanwise probability density functions of the separation shock period.

probability density functions (PDFs) of the separation shock period at various spanwise locations at 50% intermittency. The baseline curve was obtained using data taken by Erengil.[25] These PDFs are representative of those computed at other locations in the intermittent region. As f_c increases, the PDFs indicate that the separation shock motion has more short periods (i.e., higher frequency, jitter type motion). It is this increase in the high-frequency jitter motion that is responsible for the increase in the zero crossing frequency. Recall that separation shock jitter is caused by fluctuations in the instantaneous pressure ratio across the separation shock. Thus, the VGs, in addition to energizing the mean boundary layer, must also enhance turbulent fluctuations in the incoming boundary layer needed to cause fluctuations in the instantaneous pressure ratio across the separation shock. This conclusion has been confirmed with fluctuating pitot pressure measurements (not shown) that demonstrate that the pitot pressure rms in the disturbed boundary layer is substantially higher than in the undisturbed boundary layer.

Increased jitter motion is not uniform across the VG span. It can be seen in Fig. 12 that there are three PDFs at $f_c = 1.8$ kHz. The two PDFs at approximately symmetric locations about the VG apex ($Y = -0.68$ and -0.98) overlay each other. However, the PDF near the tunnel centerline ($Y = -0.076$) has a significantly higher peak at the shortest periods indicating that the separation shock has more

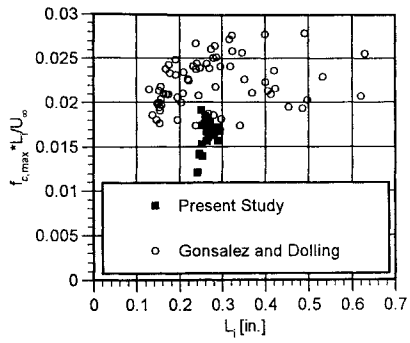

Fig. 13 Relationship between L_i and $f_{c,\max}$ in terms of Strouhal number.

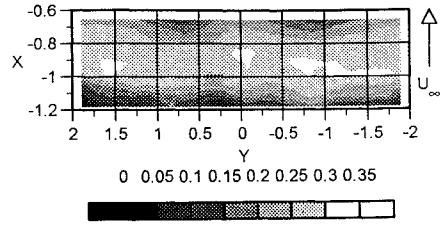

Fig. 14 Fraction of wall pressure fluctuation energy in the 100–500 Hz band in the intermittent region.

jitter at this station than at $Y = -0.86$ and -0.98. However, in order for all three of these stations to have the same zero crossing frequency (i.e., the same average period), the separation shock at $Y = -0.076$ must also have more low-frequency motions. This would suggest that there are also spanwise variations in the low-frequency separation shock motion that is caused by expansion and contraction of the separation bubble.

Gonsalez and Dolling[15] found that the intermittent region length and maximum zero crossing frequency are inversely proportional and that their relationship could be expressed in terms of a characteristic Strouhal number given by $L_i(f_{c,\max})/U_\infty$. For the boundary layer used in their study, which is essentially the same as the undisturbed boundary layer in the present study, the average Strouhal number is 0.0225 with a standard deviation of 0.00306. This relationship between $f_{c,\max}$ and L_i results from shock velocities being essentially the same in a number of different types of SWTBLIs with the same incoming boundary layer, irrespective of the intermittent region size.

Figure 13 compares the Strouhal numbers for the present study with those presented by Gonsalez and Dolling.[15] To be consistent with Gonsalez and Dolling,[15] for this figure L_i is redefined as the distance from 5% to 95% intermittency. The average Strouhal number for the present study is 0.0164, which is 2σ below that obtained by Gonsalez and Dolling.[15] Since the freestream velocities for these two studies are the same, the difference must lie in the product of $f_{c,\max}$ and L_i being less for the present study. This means that for a given L_i, on average $f_{c,\max}$ is less than that observed by Gonsalez and Dolling. This suggests that the shock velocities are lower in the disturbed interaction.

The enhanced separation shock jitter is responsible for shifting the dominant frequency band of the wall pressure fluctuations to a higher band. This shift results in reduced wall pressure fluctuation energy in the 100–500 Hz range. Figure 14 shows the distribution of the fraction of energy due to wall pressure fluctuations in the 100–500 Hz band, the typical skin panel resonant frequency band. The experimental uncertainty, based on repeated measurements, is estimated to be 7%. Like the undisturbed interaction, this distribution has a broadband peak but at a lower level. The $\beta_{\max}$, which occurs downstream of the VG apexes and along the tunnel centerline, is 0.31, an 11% decrease as compared to the undisturbed interaction. Between the centerline and VG apexes, the maximum β along a streamwise cut through the intermittent region was observed to decrease to a minimum of 0.27 (23% less than undisturbed value).

The highest zero crossing frequencies have been found in the region between the centerline and the VG apexes. It is in this region that

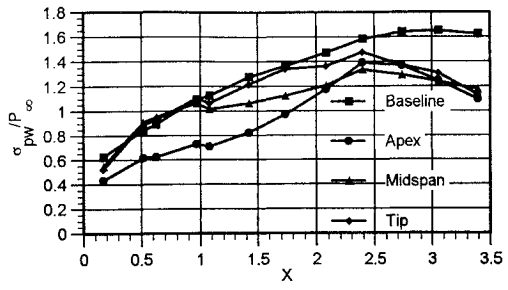

Fig. 15 Wall pressure rms distributions on the corner face.

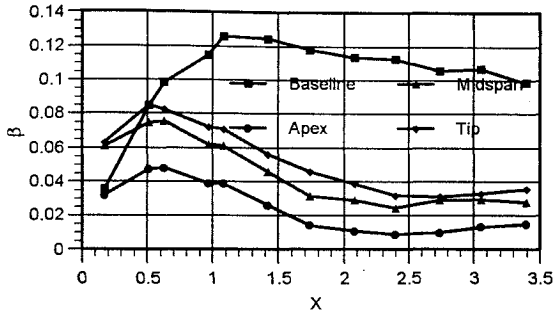

Fig. 16 Beta distributions on the corner face.

the separation shock jitter motion has been enhanced the most. Thus, the decrease in β between the centerline and apexes is consistent with the earlier discussed enhanced jitter motion of the separation shock.

Effect of VGs on Fluctuating Pressure Loads on the Corner Face

With the VGs placed upstream of the compression corner, both the magnitude of the loads and the fluctuation energy in the structural resonant frequency band are reduced. Figure 15 shows the effects of the VGs on the corner face fluctuating pressure loads. The uncertainty in σ_{pw} is estimated from repeated measurements to be 2%. The loads produced by the disturbed interaction are everywhere less than or equal to the loads produced by the undisturbed interaction. The maximum wall pressure rms (normalized by P_∞) for the undisturbed case is 1.64, and it is reduced by 10% to 1.48 by the VGs. The highest loads are found in the region immediately downstream of the VG tips which is consistent with the spanwise variation in the intermittent region length. Gramann[18] showed that as the shock moves upstream, the pressure on the corner face decreases, and as the shock moves downstream, the pressure on the corner face increases. Therefore, as the intermittent region increases in length, a point on the corner face is exposed to a greater range of pressures which causes an increase in the magnitude of the fluctuating pressure load to which that point is exposed. It was shown in Fig. 7 that the intermittent region is shortest downstream of the VG apex and longest downstream of the VG tips. Therefore, the results shown in Fig. 15 are consistent with the current understanding of the mechanism that produces loads on the corner face.

The greatest effect of the VGs is on the energy content of the loads on the corner face as seen in Fig. 16. The uncertainty in β is estimated to be 4%. Everywhere on the corner face, the amount of energy in the structural resonant frequency band is less than in the undisturbed interaction. The β_{max} is 0.13 in the undisturbed interaction but that is reduced by 35% to 0.085 by the VGs. Even more beneficial is the reduction in β near the trailing edge of the compression corner. In this region, β is reduced by 70% or more, depending on the spanwise location, which is important because it is in this region where the highest loads are found in the undisturbed interaction.

Effect of the VGs on Other Interactions

Experiments exploring the effects of the VGs on swept compression corner and unswept, blunt fin-induced interactions have recently been conducted. Results from these experiments indicate that the VGs can be effectively applied to swept interactions but not to blunt fin interactions. In swept interactions, the effects are essentially the same as those observed in unswept interactions; namely, the scale of the interaction is reduced, the magnitude of the loads is reduced, and their spectral content is shifted to a higher band. In unswept blunt fin interactions the VGs have essentially no effect on the scale of the interaction or the loads produced by it. A summary of the results from these experiments will be published in a forthcoming technical note.

Conclusions

Wheeler doublets add three dimensionality to an otherwise two-dimensional shock wave/turbulent boundary-layer interaction. The VGs reduce the magnitude of the loads and change the frequency content of separation shock-induced fluctuating pressure loads produced by compression corner induced turbulent separation. The magnitude of the maximum loading upstream of the corner was reduced by 23–29%, and the amount of energy in the low-frequency band (100–500 Hz) was reduced by 11–23%. Additionally, the area exposed to high loads is reduced by 60% due to the downstream shift of the upstream influence line. On the corner face the maximum loads are reduced by 10% and β is reduced by 35%. More importantly, near the trailing edge of the compression corner where the highest fluctuating pressure loads are found, β is reduced by 70% or more.

Pitot pressure surveys suggest that regions of the incoming boundary layer have a fuller profile. This fuller profile reduces the extent of the separated flow, which causes the interaction to shrink and the upstream influence and $\gamma = 0.99$ lines to more closer to the compression corner. Reduced loading in the intermittent region is caused by a weaker separation shock. The separation shock also has an enhanced jitter motion which shifts the frequency band of the loads to a higher band which reduces the energy levels in the skin panels' resonant frequency band.

Acknowledgments

Support for this research has been provided through a grant from NASA Langley Research Center monitored by W. E. Zorumski. Additional funding has been provided by the University of Texas at Austin through University and Thrust 2000 fellowships. The authors gratefully acknowledge this support.

References

[1]Dolling, D. S., "Fluctuating Loads in Shock Wave Turbulent Boundary Layer Interaction: Tutorial and Update," AIAA Paper 93-0284, Jan. 1993.

[2]Pozefsky, P., Blevins, R. D., and Laganelli, A. L., "Thermo-Vibro-Acoustic Loads and Fatigue of Hypersonic Flight Vehicle Structures," Air Force Wright Aeronautical Labs., AFWAL TR-89-3014, Wright-Patterson AFB, OH, Feb. 1989.

[3]Raghunathan, S., "Passive Control of Shock Boundary Layer Interaction," *Progress in Aerospace Sciences*, Vol. 25, No. 3, Pergamon, New York, 1988, pp. 271–296.

[4]Grin, V. T., and Zakharov, N. N., "Experimental Investigation of Effect of Tangential Blowing and Wall Cooling on Flow with Separation," *Fluid Dynamics*, Vol. 6, June 1974, pp. 1035–1038.

[5]Viswanath, P. R., Sankaran, L., Sagdeo, P. M., Narasimha, R., and Prabhu, A., "Injection Slot Location for Boundary Layer Control in Shock-Induced Separation," *Journal of Aircraft*, Vol. 20, No. 8, 1983, pp. 726–732.

[6]Ball, K. O. W., and Korkegi, R. H., "An Investigation of the Effect of Suction on Hypersonic Laminar Boundary Layer Separation," *AIAA Journal*, Vol. 6, No. 2, 1968, pp. 239–243.

[7]Viswanath, P. R., "Shock-Wave-Turbulent-Boundary-Layer Interaction and Its Control: A Survey of Recent Developments," *Developments in Fluid Mechanics, and Space Technology*, Indian Academy of Sciences, Bangalore, India, 1988, pp. 143–202.

[8]McClure, W. B., "An Experimental Study of the Driving Mechanism and Control of the Unsteady Shock Induced Turbulent Separation in a Mach 5 Compression Corner Flow," Ph.D. Dissertation, Dept. of Aerospace Engineering and Engineering Mechanics, Univ. of Texas, Austin, TX, Aug. 1992.

[9]Kleifges, K., and Dolling, D. S., "Control of Unsteady Shock-Induced Turbulent Boundary Layer Separation Upstream of Blunt Fins," AIAA Paper 93-3281, July 1993.

[10]Wheeler, G. O., "Means for Maintaining Attached Flow of a Flowing Medium," U.S. Patent 4,455,045.

[11]Gartling, D. K., "Tests of Vortex Generators to Prevent Separation of Supersonic Flow in a Compression Corner," M. S. Thesis, Dept. of Aerospace Engineering, Univ. of Texas, Austin, TX, 1971.

[12]Lin, J. C., Selby, G. V., and Howard, F. G., "Exploratory Study of Vortex-Generating Devices for Turbulent Flow Separation Control," AIAA Paper 91-0042, Jan. 1991.

[13]Barber, T. J., Mounts, J. S., and McCormick, D. C., "Boundary Layer Energization by Means of Optimized Vortex Generators," AIAA Paper 93-0445, Jan 1993.

[14]McCormick, D. C., "Shock-Boundary Layer Interaction Control with Low-Profile Vortex Generators and Passive Cavity," AIAA Paper 92-0064, Jan. 1992.

[15]Gonsalez, J. C., and Dolling, D. S., "Correlation of Interaction Sweepback Effects on the Dynamics of Shock-Induced Turbulent Separation," AIAA Paper 93-0776, Jan. 1993.

[16]Barter, J. W., and Dolling, D. S., "Experimental Study of the Use of Vortex Generators to Reduce Fluctuating Pressure Loads in Shock Wave Turbulent Boundary Layer Interactions," AIAA Paper 93-4335, Oct. 1993.

[17]Unalmis, O. H., and Dolling, D. S., "Decay of Wall Pressure Field and Structure of a Mach 5 Adiabatic Turbulent Boundary Layer," AIAA Paper 94-2363, June 1994.

[18]Gramann, R. A., "Dynamics of Separation and Reattachment in Mach 5 Unswept Compression Ramp Flow," Ph.D. Dissertation, Dept. of Aerospace Engineering and Engineering Mechanics, University of Texas, Austin, TX, Dec. 1989.

[19]Marshall, T., and Dolling, D. S., "Comments on the Computation of Supersonic, Unswept, Turbulent Compression Ramp Interactions," *AIAA Journal*, Vol. 30, No. 8, 1992, pp. 2056–2065.

[20]Brusniak, L., "Evaluation of Conditional Sampling Methods of Analyzing Separation Shock Motion," AIAA Paper 88-0091, Jan. 1988.

[21]Erengil, M. E., and Dolling, D. S., "Unsteady Wave Structure near Separation in a Mach 5 Compression Ramp Interaction," *AIAA Journal*, Vol. 29, No. 5, 1991, pp. 728–735.

[22]Gonsalez, J. C., "Correlation of Interaction Sweepback Effects on Unsteady Shock-Induced Turbulent Separation," M.S. Thesis, Dept. of Aerospace Engineering and Engineering Mechanics, Univ. of Texas, Austin, TX, May 1993.

[23]Settles, G. S., Vas, I. E., and Bogdonoff, S. M., "Details of a Shock-Separated Turbulent Boundary Layer at a Compression Corner," *AIAA Journal*, Vol. 14, No. 12, 1976, pp. 1709–1715.

[24]Erengil, M. E., and Dolling, D. S., "Physical Causes of Separation Shock Unsteadiness in Shock Wave/Turbulent Boundary-Layer Interactions," AIAA Paper 93-3134, July 1993.

[25]Erengil, M. E., "Physical Causes of Separation Shock Unsteadiness in Shock Wave/Turbulent Boundary-Layer Interactions," Ph.D. Dissertation, Dept. of Aerospace Engineering and Engineering Mechanics, Univ. of Texas, Austin, TX, Dec. 1993.